Stockholm University

Bachelor Thesis

Degree Project in Geology 30 hp

Zeolite mineralization associated with earthquakes in Iceland

Iliyan Deskov

Stockholm 2020

Department of Geological Sciences
Stockholm University
SE-106 91 Stockholm

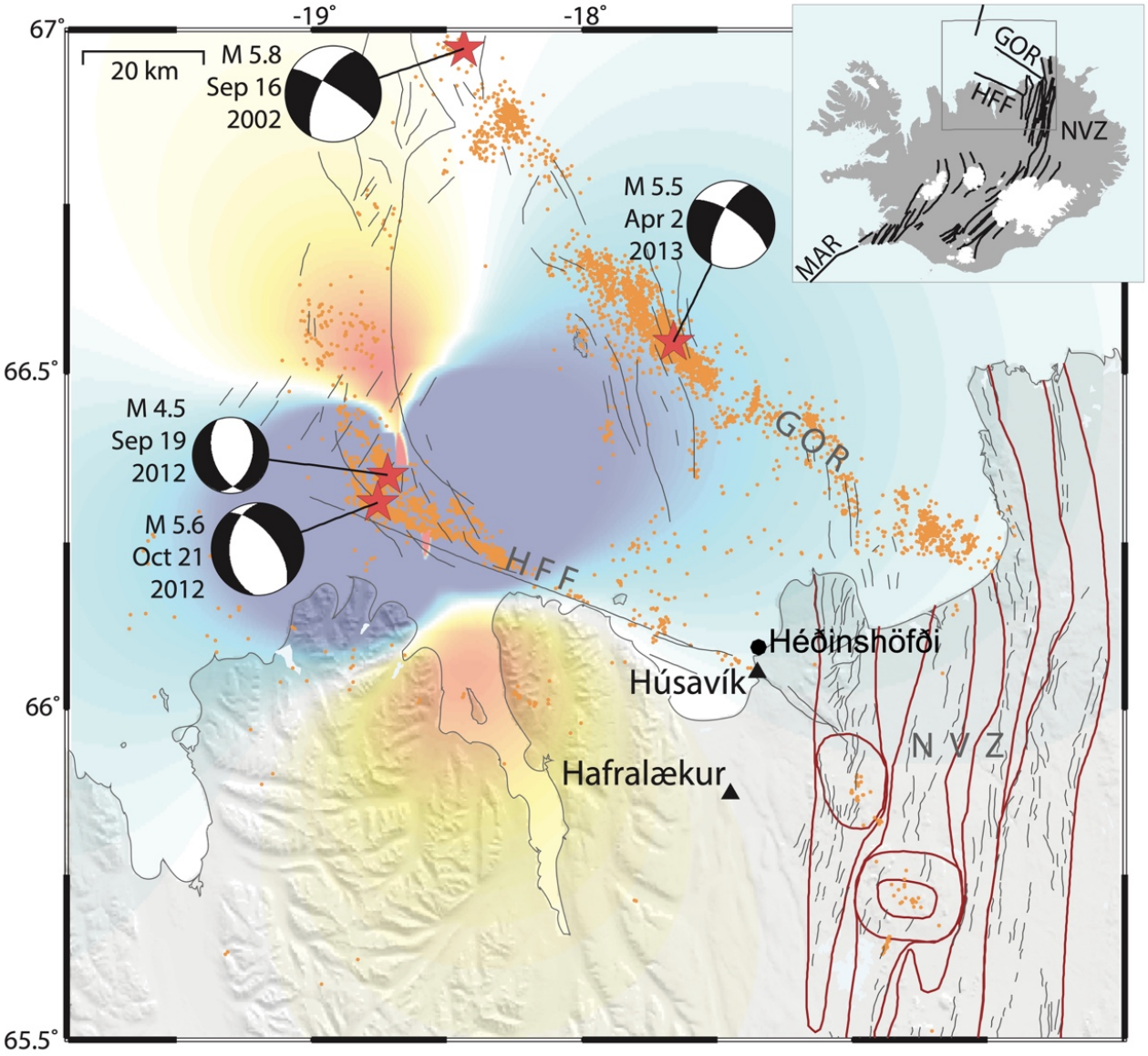

Figure 1 Map of Northern Iceland's Tjörnes Fracture Zone (TFZ). Solid red lines represent the Northern Volcanic Zone (NVZ); solid gray lines represent faults with the Húsavík-Flatey Fault (HFF) and the Grímsey Oblique Rift (GOR) marked individually. Red stars mark the epicenters of M>4.5 earthquakes. Húsavík and Hafralækur are groundwater sampling sites (previous studies); Héðinshöfði marks the location of sample collection for this study. Inset at top shows a larger view of Iceland atop the Mid Atlantic Ridge (MAR). Graphic reproduced with permission after Skelton et al., 2014.

Introduction and geologic background

Changes in groundwater chemistry have been observed before and after earthquakes in Northern Iceland and are a potentially reliable earthquake precursor signal (Andrén et al., 2016; Claesson et al., 2004; 2007; Elkhoury et al., 2006; Skelton et al., 2014; Wästeby et al., 2014). These hydrogeochemical changes probably arise from *fluid-rock* interactions during crustal dilation (mineral dissolution and re-precipitation along fractures and vesicles during fault sealing and re-fracturing), and mixing of groundwater from reservoirs with different chemistries, depths, and temperatures (Andrén et al., 2016; Claesson et al., 2004, 2007; Skelton et al., 2014; Wästeby et al., 2014).

Zeolite minerals are ubiquitous throughout the geothermally and seismically active Tjornes Fracture Zone (TFZ) of Northern Iceland – a system of transform faults connecting the offshore Kolbeinsey Ridge (KR) and Iceland's Northern Volcanic Zone (NVZ) (Drouin et al., 2017; Pedersen et al., 2009; Waltl et al., 2011). The type of zeolite forming is controlled by groundwater chemistry, pressure, and temperature (Fridriksson et al., 2001; Neuhoff, 2000; Wästeby et al., 2014) and thus zeolite mineralization should provide an independent record of seismically coupled groundwater chemistry changes at depth.

An earthquake can modify the hydrological properties of surrounding rock by changing the local stress/strain state, which changes groundwater flow patterns and/or exposes fresh rock surfaces which react with the circulating fluid (Andrén et al., 2016; Claesson et al., 2004; Elkhoury et al., 2006; Roeloffs, 1988). These processes have a direct impact on groundwater chemistry, temperature and pressure. Wästeby et al. (2014) estimate that any M>4 earthquake delivers enough seismic energy density to trigger a hydrochemical response.

Faults can act as barriers or conduits for groundwater flow. Crustal movement due to seismicity can connect or isolate chemically distinct aquifers and cause a *source switching* event (Andrén et al., 2016; Claesson et al., 2004, 2007; Evans et al., 1997; Ngwenya et al., 2000; Skelton et al., 2014), which manifests as distinct and abrupt changes in groundwater chemistry. The mechanically disturbed rock will be out of chemical equilibrium with the new fluid causing some minerals to dissolve and others to precipitate. Fault sealing typically occurs as a result of this *fluid-rock* interaction and also induces changes in groundwater chemistry, albeit much more gradual ones (Andrén et al., 2016; Claesson et al., 2004, 2007; Elkhoury et al., 2006; Wästeby et al., 2014). The relative contributions to groundwater chemistry changes from *source switching* and *fluid-rock interaction* can be inferred from the associated change in Deuterium and Oxygen-18 concentrations (Skelton et al., 2014; Claesson et al., 2004, 2007). Source switching alters ∂D concentrations while *fluid-rock* interaction affects the ^{18}O abundance in groundwater (Árnason, 1977; Claesson et al., 2007; Reddy et al., 2011; Skelton et al., 2014). This is because hydrogen is far less abundant in the rock chemistry (~1 weight %) as compared to ~46 weight % for oxygen (Cole et al., 1987).

Some researchers argue that the processes leading up to and following an earthquake leave specific chemical markers in the groundwater (Kagan, 2007; Roeloffs, 1988; Skelton et al., 2014; Thomas, 1988; Wästeby et al., 2014). Significant (12-19%) increases in the concentrations of B, K, Li, Mo, Na, Rb, S, Si, Sr, Ca, Cl and SO_4 occurring 1, 2, 5 and over 10 weeks *before* a M>5 earthquake were reported by Claesson et al. (2004, 2007). They argue that the initial changes were caused by the rupturing of a

hydrologic barrier between two chemically distinct aquifers. They further argue that subsequent chemical recovery to pre-earthquake levels was most likely controlled by progressive isolation of the two aquifers by zeolite mineralization along groundwater flow paths. Abrupt increase of Na and Ca concentrations *prior* to two consecutive M>5 earthquakes was reported by Andrén et al. (2016) and Skelton et al. (2014) with the former attributing the jump in Na concentration to a shift away from chemical equilibrium leading to the non-stoichiometric release of Na from analcime (a Na bearing zeolite) possibly due to an increase of active surface area caused by fracturing and/or to mixing of chemically distinct groundwater components. This interpretation is consistent with earlier ones by Skelton et al. (2014) where groundwater chemistry was reported to change significantly 4 – 6 months *prior* to two M>5 earthquakes. Based on hydrogeochemical modelling and petrological evaluation Skelton et al. (2014) show that zeolites observed along cracks and vesicles of their rock samples are saturated in the circulating fluid, suggesting that groundwater chemistry is a key control on zeolite mineralization. Those authors also statistically confirm that changes in groundwater chemistry are uniquely related to seismic events and not part of a random distribution.

Zeolite assemblages represent a sensitive geologic record of temperature and pressure conditions, and of groundwater chemistry in the crust (Fridrikson et al., 2001; Neuhoff et al., 2000; Wästeby et al., 2014). Zeolites are tectosilicates characterized by open frameworks of Si and Al tetrahedra enclosing channels containing charge balancing cations of alkali and alkaline-earth metals, as well as molecular water (Neuhoff et al., 2000). They are common hydrothermal alteration products in volcanic rocks (Andrén et al., 2016; Gottardi and Galli, 1985; Gottardi, 1989; Skelton et al., 2014, 2016; Wästeby et al., 2014). Owing to their high cation exchange capacities their mineralization causes significant changes in the ion content of groundwater (Neuhoff et al., 2000). Formation of zeolites has been shown to reduce porosity and limit, or completely seal, pathways for groundwater flow, which can have fundamental effects on water chemistry (Claesson et al., 2004, 2007; Neuhoff et al., 2000). Zeolite (and other minerals) mineralization is a major actor in post-seismic fault healing (Claesson et al., 2004; Wästeby et al., 2014).

The study presented here evaluates whether zeolite mineralization provides an independent record of groundwater chemistry at depth. More specifically, we identify primary and secondary minerals in rock samples; propose a mineral reaction pathway by which secondary minerals form, and discuss this reaction's effect on groundwater chemistry.

Mineral identification was done by X-ray diffractometry (XRD) and optical microscopy; X-ray fluorescence spectroscopy (XRF) was used for bulk chemical analysis. Water chemistry data was used from the published literature, e.g. Andrén et al., 2016; Claesson et al., 2004, 2007; Skelton et al., 2014; Wästeby et al., 2014. Rock samples were collected at Héðinshöfði (66.096150ºN, 17.34419ºW) (See Fig. 1), a marine headland about 6 km north of Húsavík where a normal fault has brought rocks from a depth of about 1000 m to the surface. These are hydrothermally altered basaltic lava flows where zeolites filling cracks and vesicles are preserved and can therefore be studied in rock samples (Wästeby et al., 2014).

This work is carried out under the broader umbrella of earthquake forecasting through collection and interpretation of hydrogeochemical precursors and their associated effects on mineralogy. Numerous studies have reported precursory hydrogeochemical changes (Andrén et al., 2016; Claesson et al., 2004; Roeloffs, 1988; Skelton et al., 2014; Thomas, 1988). The problem with earthquake forecasting is the sheer number of phenomena occurring around a seismic event, which makes it extremely difficult to

distinguish a method with real predictive potential from a forecasting method that owes its efficacy to coincidence (Kagan, 1997). One possible exception is the study conducted by Skelton et al., (2014) who were able to statistically prove probable association between precursory hydrogeochemical activity and two M 5–6 earthquakes on 21 October 2012 and 2 April 2013, respectively.

Methods

Rock samples were collected on 29 June 2018 from the damage zone of the HFF, which is exposed and accessible at Héðinshöfði (See Fig. 1). Rock chips for thinsections were cut by the author at Creative MicroSystems Corporation (CMC) in Vermont using a diamond-blade rock saw. From these chips 6 thin sections were produced by Vancouver Petrographic in British Columbia, Canada. Powders for XRD and XRF analysis were crushed in a vise and manually sorted under an inspection microscope so as to separate paler from darker ground mass and both ground masses from the zeolite vesicle material. The three constituents were weighed using a Sartorius type 1801 laboratory scale with a 0.1 mg accuracy and then powdered. X-ray diffraction data were collected from these powders using a Rigaku Miniflex II X-ray diffractometer with a monochromator (kß filter) on zero-background sample holders. The diffractometer's goniometer was calibrated to 0.001° accuracy. Data were analysed using Rigaku's PDXL software version 1.6.0.0.

A Hitachi X-Met8000 Expert Geo X-ray fluorescence spectrometer was used for bulk chemical analysis of the powder samples used for XRD analysis. The limit of detection for most transition metals is in the 5-10 ppm range (0.0005% to 0.001%), with Na being too light and below this limit and therefore undetected (Hitachi High-Tech Analytical Science, 2017). All X-ray work and petrographic investigations were done at the University of Vermont's Department of Geology in Burlington, Vermont USA.

Our conceptualization of the fluid-rock system assumes preservation of mass balance between rock and groundwater where primary phases in the matrix (olivine, plagioclase, pyroxene, basaltic glass and various Fe/Ti oxides) react with groundwater, some are dissolved, releasing elements which were carried away by the fluid while others (zeolites, clays) precipitate along cracks and inside vesicles from solution in groundwater consuming some combination of elements. Both processes produce a chemical signal that can be recorded at hydrogeochemical sampling sites. It is this chemical signal that is of interest to us and thus we propose a general metamorphic reaction, which relates element concentrations in the apparently unaltered 'light matrix' to element concentrations in the more altered 'dark matrix', vesicle material and ultimately the groundwater.

$$Ci(light\ matrix) = x.Ci\ (vesicle) + (1-x).Ci(dark\ matrix) + y.Ci(groundwater)$$

where y is the contribution to groundwater concentrations of the respective element (the value in column E of Table 2); Ci is the concentration of element i. And x is a mass fraction of the respective sample, $x = \frac{mass\ of\ vesicle}{mass\ of\ vesicle + mass\ of\ dark\ matrix} = \frac{1.351}{1.351+0.74} = 0.646$

The same equation rearranged for groundwater concentration:

$$y.Ci(groundwater) = Ci(light\ matrix) - [\, x.Ci\ (vesicle) + \ (1 - x).Ci(dark\ matrix)]$$

Results

Rock samples exhibit three distinct regions (Fig. 2) – a pale colored general basaltic matrix; dark colored veins and rims; and milky white zeolite-filled vesicles. All vesicles are rimmed and interconnected by the dark veins and both are hard and brittle, while the primary matrix is softer and easily broken.

Petrographic examination of the six thin sections reveals an extensively altered, fine grained primary basaltic matrix of mostly pyroxenes and plagioclase with occasional olivine (*Figures 2 - 5*). Vesicles and fractures contain several generations of zeolites with amorphous iron oxides/hydroxides often lining vesicle walls and/or appearing as small opaque inclusions (*Figures 4 & 5*). The zeolites show large variability in crystal size – from large euhedral crystals to very fine grained aggregates; and habit – ranging from massive to tabular to radiating. Some areas contain calcite alongside iron oxides and the zeolites. Numerous micro-cracks and fractures are visible in all 6 thin sections. In most cases, multiple generations of secondary minerals have filled and sealed these fractures.

Eight diffraction patterns were obtained identifying 13 crystalline phases with the mineralogies of the 3 distinct rock regions shown in Table 1. These regions are: *(i)* minimally altered primary basaltic matrix (pale-colored); *(ii)* strongly altered matrix lining the outsides of all vesicles and cracks (dark-colored); and *(iii)* vesicle material – white with numerous rust-colored stains. Calcite was detected only once by XRD. Table 2 shows the bulk chemistry of the same 3 regions obtained by XRF.

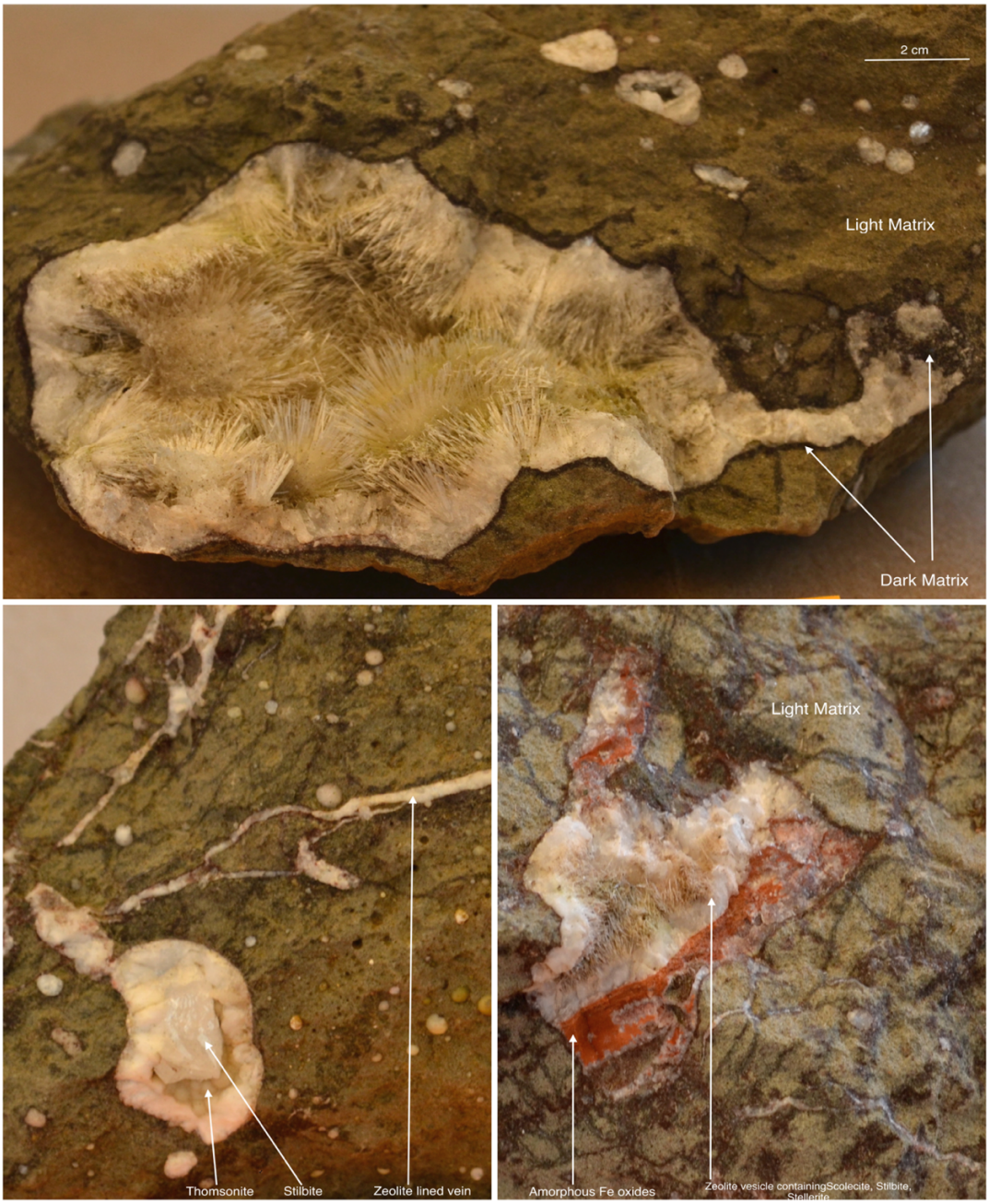

Figure 2 Photographs of rock samples. Clearly visible are the minimally altered Light Matrix cut by a network of veins of the more altered Dark Matrix. Top image shows a large vesicle filled with different generations and habits of zeolite minerals.

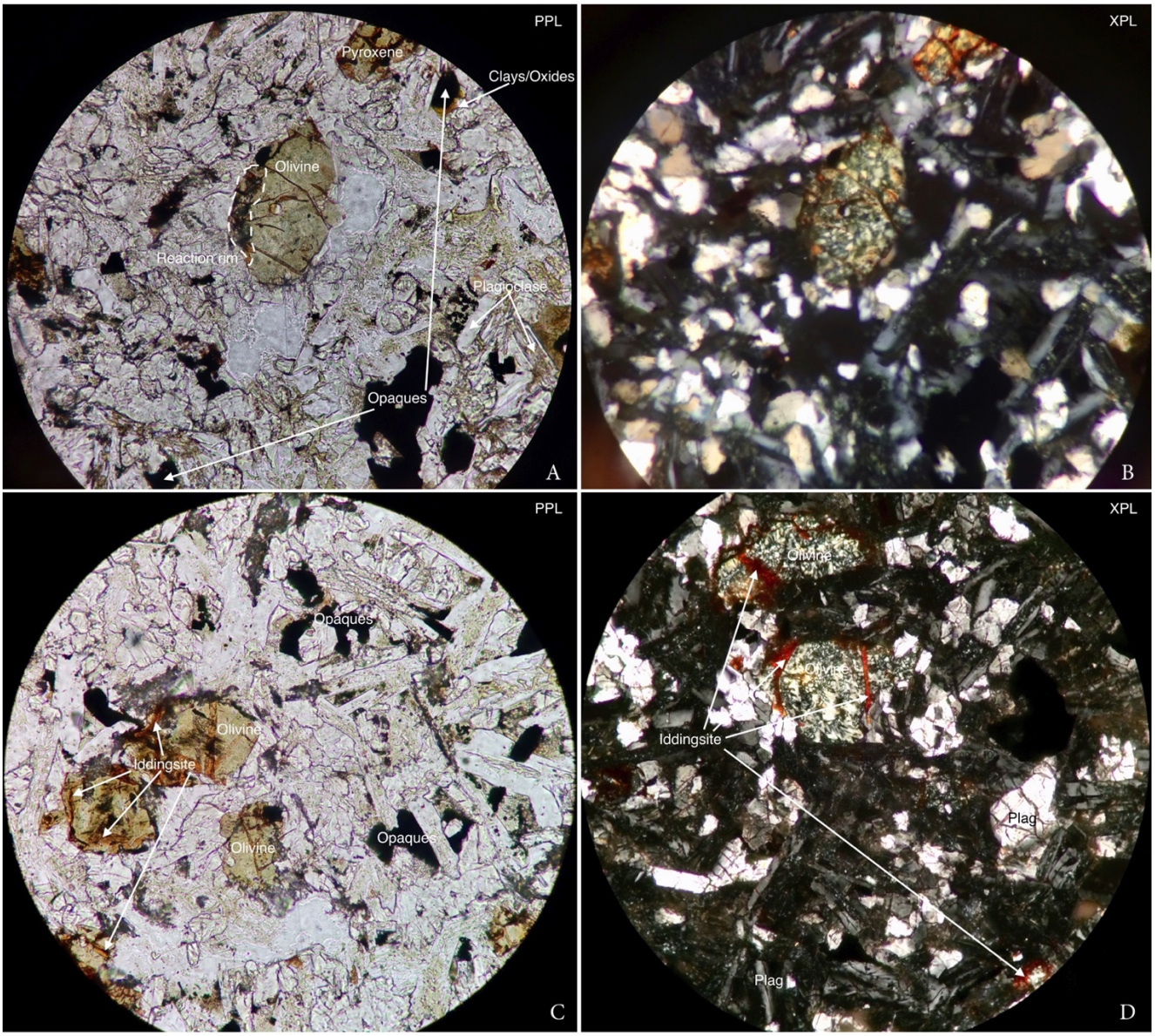

Figure 3 Photomicrographs of thinsections from Héðínshöfði. A large olivine phenocryst is visible in A(PPL) and B(XPL); it is extensively fractured and altered. Strong iddingsitization of another olivine crystal observed in C (PPL) and D (XPL). Numerous rounded opaque grains visible in all images. (80X Magnification)

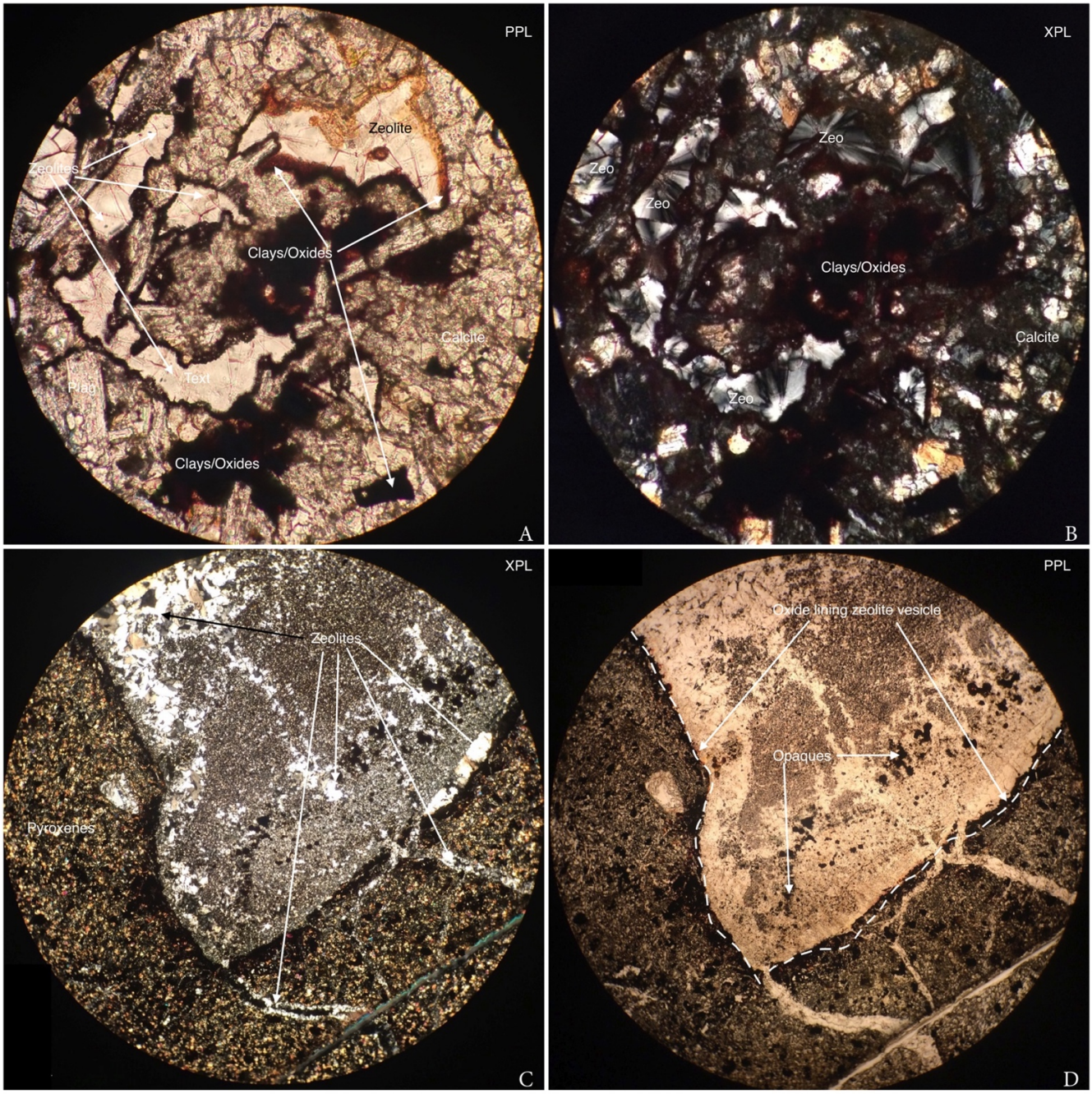

Figure 4. Several angular zeolite crystals, clays and muds, calcite, and highly altered primary plagioclase in PPL (A) and XPL (B). Images C and D are of the same spot showing the rim of a zeolite vesicle in XPL(C) and PPL (D). Note the colorful primary fine grained pyroxenes and secondary zeolites dotted with opaque Fe or Fe/Ti oxides in D. (40X Magnification)

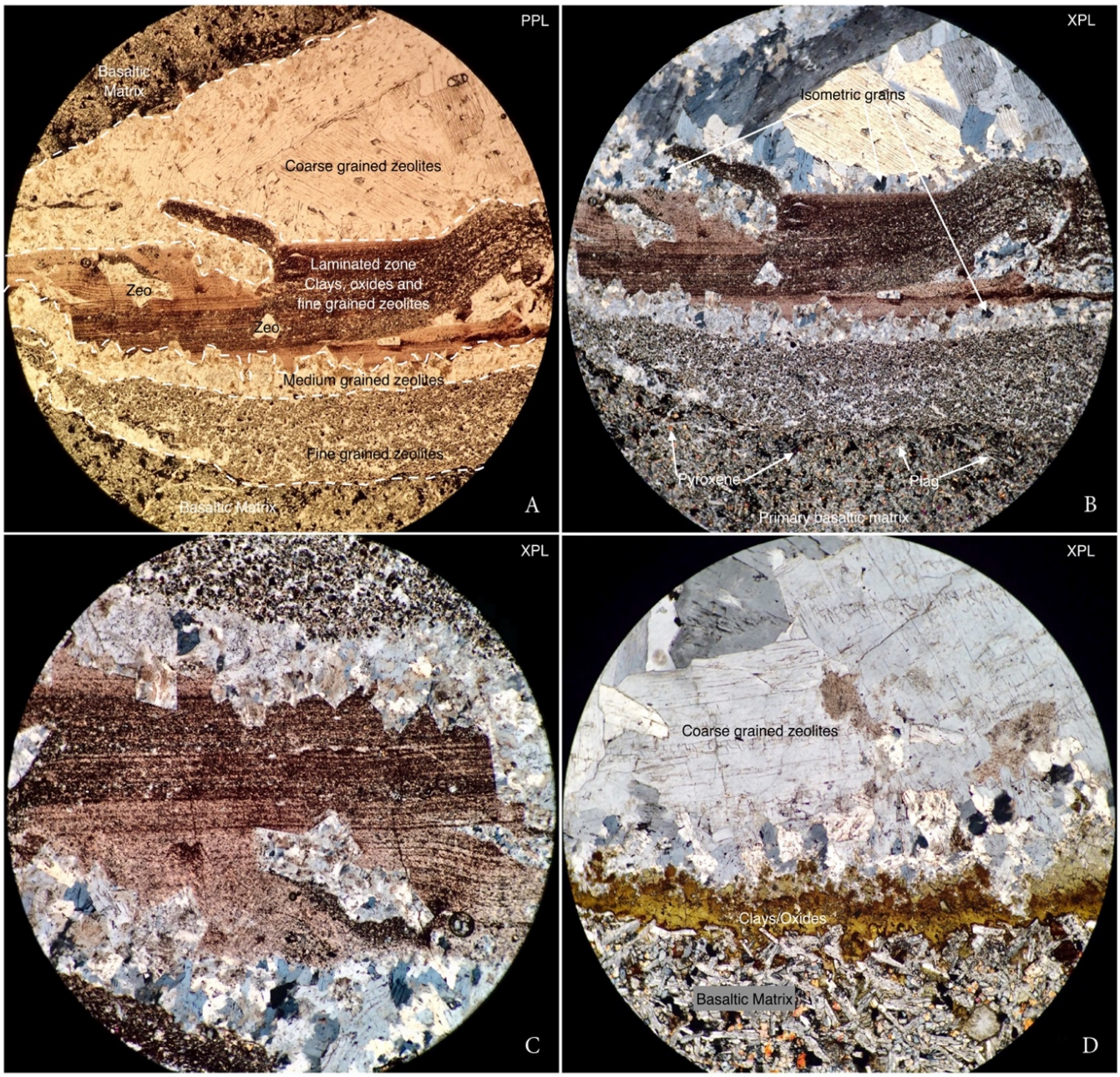

Figure 5. Various layered structures in zeolite filled vesicles. Image A shows a succession of contacts between the original basaltic rock (bottom) a first generation fine grained zeolite (above lowest dashed line), a second generation of a medium grained zeolite (above second lowest dashed line), laminated clays, muds and oxides above that and another generation of well formed, coarse grained zeolite in contact with the original basaltic rock (under top dashed line). B shows A but in XPL.
Image C shows several contacts between matrix, zeolite and clays which appear to be fractured (vertical lines around the center of image). Image D shows a clay/oxide margin between the original basaltic body and a well formed zeolite filling a vesicle. (A,B and C at 40X; D at 80X magnification)

Mineral	Light Matrix	Dark Matrix	Zeolite Vesicle
Diopside (Di) $Ca_{0.87}\,Fe_{0.19}\,Mg_{0.94}\,Si_2\,O_6$	*		
Albite, calcian (Ab) $Ca_{0.32}\,Na_{0.68}\,Al_{1.46}\,Si_{2.54}\,O_8$	*		
Ferrosilite, magnesian (Fs) $Ca_{0.16}\,Fe_{0.67}\,Mg_{0.32}\,Si\,O_3$		*	
Anorthite (An) $Ca_{0.9}\,Na_{0.1}\,Al_2\,Si_2\,O_8$		*	
Clinochlore (Chl) $Fe_{0.4}\,Al_{0.6}\,Mg_4\,Si_{2.5}\,Al_{1.5}\,O_{10}$		*	
Thomsonite-Ca, (Tho) $Ca_2\,Na\,Al_5\,Si_5\,O_{20}$		*	
Natrolite (Nat) $Ca_{0.04}\,Na_{1.96}\,Al_{2.04}\,Si_{2.96}\,O_{10}$		*	
Scolecite (Sco) $Ca\,Al_3\,Si_3\,O_{10}$		*	*
Calcite (Cal) $CaCO_3$			*
Laumontite (Lau) $CaAl_2Si_4O_{18}$			*
Stellerite (Ste) $Ca_2\,Al_4\,Si_{14}\,O_{36}$			*
Stilbite-Ca (Sti) $Ca_4\,Na_{0.72}\,Al_{10}\,Si_{26}\,O_{72}$			*

Table 1. XRD results showing mineral distribution between the 3 distinct rock regions.

Table 2 below lists XRF data showing relative element abundance in the three rock regions (Na is too light and thus its concentration is below the detection threshold of our equipment). Columns B, C and D list concentrations of each element in each of the respective samples. Column E lists a calculated concentration in groundwater based on data from columns B, C, and D using the equation from the Methods section:

$$y.Ci(groundwater) = Ci(light\ matrix) - [\,x.Ci\,(vesicle) + (1-x).Ci(dark\ matrix)]$$

Our general model assumes that whatever set of mineral reactions takes place during the alteration of primary basalt and the production of zeolites is recorded in and can be fully described from the final mineral assemblage (XRD) balanced against the bulk chemistry of the same samples (XRF). If mass balance is maintained between rock and fluid, then original material chemistry minus secondary material chemistry should equal the system's contribution to groundwater chemistry.

(A) Element (%)	(B) Light Matrix	(C) Dark Matrix	(D) Zeolite Vesicle	(E) Contribution to groundwater
Al	5.79	8.52	6.11	-1.173
Mg	2.55	4.46	2.84	-0.863
Si	19.86	22.27	18.99	-0.291
Zr	0.01	0.01	0.02	-0.006
Na	0	0	0	0.000
Ni	0.02	0.01	0.01	0.010
Zn	0.02	0.01	0.01	0.010
Cr	0.03	0	0.03	0.011
Sr	0.03	0.01	0.02	0.014
Cu	0.03	0	0.02	0.017
Mn	0.26	0.13	0.25	0.052
P	0.28	0.07	0.31	0.055
V	0.23	0	0.24	0.075
Ba	0.12	0	0.02	0.107
K	0.35	0	0.27	0.176
Ti	1.07	0.68	1.01	0.177
Ca	8.34	6.4	9.36	0.028
Fe	15.54	8.44	15.47	2.559

Table 2. Elemental abundance data (XRF) obtained from the three distinct constituents. Column E lists a calculated value based on the method discussed in the text. Same column is colored to highlight the predicted absence (green) and over-abundance (red) of an element.

DISCUSSION

We base the discussion of our chemical system on three main data sources - bulk chemistry data (XRF), mineralogy and crystal chemistries (XRD) and previously published hydrogeochemical data (Andrén et al., 2016; Claesson et al., 2004, 2007; Skelton et al., 2014; Wästeby et al., 2014). X-ray diffraction scans

have given us a good estimate for most of the detected crystalline phases' chemistries. Petrographic thin section observations provide a fourth data stream used to evaluate the plausibility of our assertions.

Bulk chemistry data are presented in Table 2 which lists the concentration of each detected element in weight percent. Column E of that table displays a calculated groundwater concentration for each element as a result of the mineral reaction described in the Methods. The values in column E are arrived at by solving the mass balance equation for y using data from columns B, C, and D.

$$y.\mathrm{C}i(groundwater) = \mathrm{C}i(light\ matrix) - \{x.\mathrm{C}i(vesicle) + (1-x).Ci(dark\ matrix)\}.$$

Based on this calculation four elements stand out in column E of Table 2 – Al, Mg, and Si because of their apparent negative groundwater concentration and Fe – because of its strongly positive one. We take this fact to mean that some proportions of the first three elements are missing from the original Light Matrix chemistry, probably due to late magmatic, early deuteric or metamorphic reactions with groundwater, which has resulted in dissolution and removal of primary phases, such as olivine. In order to correct for this apparent lack, we add olivine to the general mass balance equation as follows:

$$\mathrm{y}.\mathrm{C}i(groundwater) = \{\mathrm{C}i(light\ matrix) + Ol + Plag + Px\} - \{x.\mathrm{C}i(vesicle) + (1-x).Ci(dark\ matrix)\}$$

Phase Name	Moles	Ca	Na	Fe	Mg	Al	Si	O
Reactant								
Diopside	4.00	0.87		0.19	0.94		2.00	6.00
Albite	12.00	0.32	0.68			1.46	2.54	8.00
Anorthite	10.00	0.90	0.10			2.00	2.00	8.00
Ferrosillite	3.00	0.16		0.67	0.32		1.00	3.00
Olivine*	5.00	0.04		0.42	1.50	0.04	1.00	4.00
Sums of reactant		17.00	9.16	4.87	12.21	37.72	66.48	229.00
Product								
Thomsonite	2.00	2.00	1.00			5.00	5.00	20.00
Clinochlore	3.00			0.40	4.00	2.10	2.50	10.00
Scolecite	1.00	1.00				2.00	3.00	10.00
Natrolite	1.00	0.04	1.96			2.04	2.96	10.00
Stilbite	1.00	4.00	0.72			10.00	26.00	72.00
Stellerite	1.00	2.00				4.00	14.00	36.00
Laumontite	1.00	1.00				2.00	4.00	18.00
Sums of product		12.04	4.68	1.20	12.00	36.34	67.46	216.00
Reactants minus products		4.96	4.48	3.67	0.21	1.38	-0.98	13.00

*Table 3. Table laying out the balanced reaction between primary phases, groundwater and secondary products. * indicates that mineral has been added to the chemistry but not observed with XRD.*

The addition of primary olivine is consistent with our thin section observations where that mineral is present and extensively altered. Our XRD scans did not identify any olivine so an average Icelandic basalt composition of $Fo_{74}Fa_{26}$ was used (Hollocher, 2019; Heirer et. al., 1966).

Table 3 lays out a mechanism for balancing a proposed fluid-rock reaction set using all phases we identify by XRD with added olivine and artificially increased abundances of pyroxene and plagioclase. The yellow columns list a number of moles of each participating phase. Each horizontal row represents an unique mineral. The number of moles from the yellow column are multiplied by the relative abundance (from XRD) of each element in each phase and then summed. The sums are calculated individually for reactants (in row name 'Sums of reactant') and products (in row name 'Sums of product') and the difference between the two is listed in the bottom row of the table.
The function of this table is to calculate and balance a number of moles of primary minerals required to produce a number of moles of secondary minerals and what left-over dissolved ionic load is released to the groundwater that agrees with modern-day groundwater chemistry data (Andrén et al., 2016; Claesson et al., 2007; Skelton et al., 2014).

Magnesium concentrations are reported to be nearly constant through time (e.g. Claesson et al., 2007, Figure 4; Wästeby et al., 2016, Figure 5a) therefore our ratio of reactants to products in Table 3 was chosen such that as a result of the reaction Mg concentration remains relatively unchanged. The resulting effect on groundwater chemistry is that Ca, Na, Fe and Al are added to it (moles listed in bottom row); and Si is taken up from solution. This means that after the addition of 5 moles of olivine, 22 moles of plagioclase and 7 moles of pyroxene to the original mineral assemblage there is an excess of Ca, Na, Fe and Al in the reactants as compared to the products; Mg is even; and that Si is insufficient in the reactants to allow the formation of all the products. This apparent lack of Si could mean that silica or quartz is also in the reactants or, alternatively, excess silica needed for the formation of our proposed products is supplied by the circulating fluid from a previous reaction stage and not by the dissolution of any primary minerals (see Andrén et. al., 2016, Figure 4).

Based on data from Table 3 a metamorphic reaction can be written as:

$$4Di + 12Ab + 10An + 3Fs + 5Ol \rightarrow 2Th + 3Chl + 1Sco + 1Nat + 1Stil + 1Ste + 1Lau + Ca + Na + Fe + Al.$$

The above reaction indicates that Ca, Na, Fe and Al are released into groundwater (see Table 3). This prediction is consistent with reported Ca and Na groundwater data (Claesson et. al., 2004; Skelton et. al., 2014) but the ratio between the two in our case is ~1 while Claesson et. al. (2004) reports Na/Ca ratios between 3.3 and 3.4.

Lastly, our mineral reaction suggests a strong increase of Fe concentration in groundwater, but this observation is not consistent with the published groundwater chemistry data (Andrén et al., 2016; Claesson et al., 2004, 2007; Skelton et al., 2014; Wästeby et al., 2014), where Fe content and behaviour are similar to that of Mg.

We argue that iron oxides and hydroxides are precipitates of a separate reaction unrelated to the one describing the formation of zeolites and possibly associated with the magnetite-quartz-fayalite-

laumontite buffer system described by Neuhoff et. al. (2000). Table 2 shows a predicted release of K, which coupled with the presence of layered clays/muds rimming zeolite vesicles suggests that Fe may be taken up in K-rich precipitates combining potassic clays and iron oxides and/or oxyhydroxides (See Figures 1 and 4). Opaque phases are ubiquitous in all thin section images, but it is unclear whether these are secondary Fe/Ti precipitates or primary glass or Fe oxides which are supplying the excess Fe. The precipitation of oxyhydroxides of Fe and Ti in a separate reaction chain could also explain the fate of the excess oxygen liberated from the zeolite forming reaction. Our calculations suggest that 5 moles of O and 3.67 moles of Fe are unaccounted for. This is a O/Fe ratio of ~1.36 which is very near the O/Fe ratio of magnetite (Fe_3O_4), which is 1.3. Magnetite was not detected by XRD but is suspected in thin section.

Conclusions

- Adding olivine, plagioclase and pyroxene to the primary mineral assemblage has provided enough 'raw material' (moles of primary minerals) to produce a plausible combination of the observed secondary minerals (alteration products) and to provide 'left over' dissolved ions necessary to produce hydrogeochemical changes consistent with present day observations.

- The behavior of Iron remains unexplained by our model. We suspect that element is participating in an unrelated set of reactions whereby primary olivine and pyroxenes are dissolving and providing feedstock for the formation of secondary phases, but Iron is either not being taken up in crystalline products or its oxides and oxyhydroxides are precipitating in Potassium rich clays and muds, which were observed in thin section but difficult to detect with XRD without special sample preparation. Opaque Iron-bearing inclusions were numerous in thin section. This could mean that the formation of (amorphous) Iron oxides and oxyhydroxides are consuming any Iron released from primary phases.

- Finally, if further exploration of the connections between zeolite mineralization, associated groundwater chemistry changes and earthquakes were needed, a more sophisticated data gathering and analysis methodology and more accurate chemical analyses such as Electron Probe Micro Analyzer (EPMA) scans of thin sections may be necessary. Whole rock XRD should also be carried out in order to determine exact proportions of minerals making up the rock body.

References

Andrén, M. *et al.* (2016) 'Coupling between mineral reactions, chemical changes in groundwater, and earthquakes in Iceland', *Journal of Geophysical Research: Solid Earth*, 121(4), pp. 2315–2337. doi: 10.1002/2015JB012614.

Árnason, B. (1977) Hydrothermal systems in Iceland traced by deuterium. *Geothermics* 5, 125–151.

Claesson, L. *et al.* (2004) 'Hydrogeochemical changes before and after a major earthquake', *Geology*, 32(8), pp. 641–644. doi: 10.1130/G20542.1.

Claesson, L., Skelton, A, Graham, C., Mörth, C.M. (2007) 'The timescale and mechanisms of fault sealing and water-rock interaction after an earthquake', *Geofluids*, 7(4), pp. 427–440. doi: 10.1111/j.1468-8123.2007.00197.x.

Cole, D.R., Mottl, M.J., Ohmoto, H. (1987) 'Isotopic exchange in mineral-water systems. II. Oxygen and hydrogen isotopic investigation of the experimental basalt-seawater system.' *Geochimica et Cosmochimica Acta*, 51, 1523–38.

Drouin, V. *et al.* (2017) 'Deformation in the Northern Volcanic Zone of Iceland 2008–2014: An interplay of tectonic, magmatic, and glacial isostatic deformation', *Journal of Geophysical Research: Solid Earth*, 122(4), pp. 3158–3178. doi: 10.1002/2016JB013206.

Elkhoury, J. E., Brodsky, E. E. and Agnew, D. C. (2006) 'Seismic waves increase permeability', *Nature,* 441(June). doi: 10.1038/nature04798.

Evans, J. P., Forster, C. B. and Goddard, J. V. (1997) 'Permeability of fault-related rocks, and implications for hydraulic structure of fault zones', *Journal of Structural Geology*, 19(11), pp. 1393–1404. doi: 10.1016/S0191-8141(97)00057-6.

Fridriksson, T., Neuhoff P.S., Arnórsson, S., Bird, D.K. (2001) 'Geological constraints on the thermodynamic properties of the stilbite-stellerite solid solution in low-grade metabasalts', *Geochimica et Cosmochimica Acta*, 65(21), pp. 3993–4008. doi: 10.1016/S0016-7037(01)00629-9.

Gottardi G. (1989) 'The genesis of zeolites.' *European Journal of Mineralogy* 1, 479–487.

Gottardi G. and Galli E. (1985) 'Natural zeolites.' Springer-Verlag.

Hitachi High-Tech Analytical Science (2017), Application note – 26, http://www.ndtproducts.ca/products/files/HHAX-MET8000Application-Note-On-site-contaminants-screening-in-soil.pdf (accessed February 2020).

Kagan, Y. Y. (1997) 'Are earthquakes predictable?', *Geophysical Journal International*, 131(3), pp. 505–525. doi: 10.1111/j.1365-246x.1997.tb06595.x.

Neuhoff P. S. (2000) 'Thermodynamic Properties and Parageneses of Rock-Forming Zeolites.' Doctoral thesis, Stanford University.

Neuhoff, P. S., Fridriksson, T., Bird, D.K. (2010) 'Zeolite Parageneses in the North Atlantic Igneous Province : Implications for Geotectonics and Groundwater Quality of Basaltic Crust', *International Geology Review, Vol. 42, 15-44.* doi: 10.1080/00206810009465068.

Ngwenya, B. T., Elphick, S.C., Main, I.G., Shimmield, G.B. (2000) 'Experimental constraints on the diagenetic self-sealing capacity of faults in high porosity rocks', *Earth and Planetary Science Letters*, 183(1–2), pp. 187–199. doi: 10.1016/S0012-821X(00)00261-2.

Pedersen, R., Sigmundsson, F. and Masterlark, T. (2009) 'Rheologic controls on inter-rifting deformation of the Northern Volcanic Zone, Iceland', *Earth and Planetary Science Letters*. Elsevier B.V., 281(1–2), pp. 14–26. doi: 10.1016/j.epsl.2009.02.003.

Reddy, D. V., Nagabhushanam, P. and Sukhija, B. S. (2011) 'Earthquake (M 5.1) induced hydrogeochemical and δ18O changes: Validation of aquifer breaching-mixing model in Koyna, India', *Geophysical Journal International*, 184(1), pp. 359–370. doi: 10.1111/j.1365-246X.2010.04838.x.

Roeloffs, E. A. (1988) 'Hydrologic precursors to earthquakes: A review', *Pure and Applied Geophysics PAGEOPH*, 126(2–4), pp. 177–209. doi: 10.1007/BF00878996.

Skelton, A. *et al.* (2014) 'Changes in groundwater chemistry before two consecutive earthquakes in Iceland', *Nature Geoscience*, 7(10), pp. 752–756. doi: 10.1038/NGEO2250.

Thomas, D. (1988) 'Geochemical precursors to seismic activity', *Pure and Applied Geophysics PAGEOPH*, 126(2–4), pp. 241–266. doi: 10.1007/BF00878998.

Waltl, P. *et al.* (2011) 'The Geological and Urban Setting of Húsavík , North Iceland , in the Context of Earthquake Hazard and Risk Analysis', pp. 1–3. *Second European Conference on Earthquake Engineering and Seismology, Istanbul, August 25-29, 2014*.

Wästeby, N. et al. (2014) 'Hydrochemical monitoring, petrological observation, and geochemical modeling of fault healing after an earthquake', *J. Geophys. Res. Solid Earth*, 119, doi:10.1002/2013JB010715.